Supplementary information for

Unappreciated role of sulfate radicals in the aqueous aging process of methoxyphenols derived from biomass burning

Ru Chen[1], Xiang Li[1], Xinjiao Huang[1], Yanli Ge[2,*], Ruiyu Li[3,4], Tianzeng Chen[3,4], Zhengzheng Yang[1], Lu Fan[1], Mingchao Sun[1], and Changgeng Liu[1,*]

[1]College of Chemistry and Materials Science, Sichuan Normal University, Chengdu 610066, China

[2]State Environmental Protection Key Laboratory of Quality Control in Environmental Monitoring, China National Environmental Monitoring Centre, Beijing, 100012, China

[3]Laboratory of Atmospheric Environment and Pollution Control, Research Center for Eco-Environmental Sciences, Chinese Academy of Sciences, Beijing 100085, China

[4]University of Chinese Academy of Sciences, Beijing 100049, China

*Corresponding author.

E-mail address: Yanli Ge (geyl@cnemc.cn) and Changgeng Liu (changwyx@sicnu.edu.cn)

This file includes:

Number of pages: 18

Number of text sections: 7

Number of figures: 8

Supporting references

1 Chemicals

Vanillic acid (VAA, >98%), vanillin (VAL, >99%), coniferyl aldehyde (CFA, >98%), sodium persulfate ($Na_2S_2O_8$, PDS, >98%), ferulic acid (FA, >99%), ethanol (≥99.8%), 5,5'-dithiobis (2-nitrobenzoic acid) (DNTB) and *tert*-butyl alcohol (TBA, ≥99%) were supplied by Aladdin. Dichloromethane (CH_2Cl_2, >99.9%), disodium hydrogen phosphate anhydrous, sodium dihydrogen phosphate dihydrate were from Chronchem. *N,O*-bis (trimethylsilyl) trifluoroacetamide (BSTFA) and dithiothreitol (DTT) were purchased from Macklin. All chemicals were used as received without further purification.

2 Possible effects of temperature and ion strength

Ionic strength in this system was in the range of 0.15 M to 0.3 M, calculated on the basis of 50 mM $Na_2S_2O_8$ and 100 mM Na_2SO_4, respectively. Under typical atmospheric conditions, ionic strength of sulfate in aerosol water are high (e.g., >4 M at less than 80% relative humidity) (Cope et al., 2022), which is much higher than that in this work. Therefore, the potential effect of ionic strength on the reactions might be not important and not considered in this work.

Thermal activation of PDS was employed to generate $SO_4^{\bullet-}$ in this work, which has been demonstrated to be effective for $SO_4^{\bullet-}$ production and is suitable for long-term experimental simulation studies (Herrmann et al., 2010, 2015). Although the temperature (50 °C) used in this work is higher than typical ambient conditions, previous studies have reported that the total rate constants for the reactions of 2-

methoxyphenol and 2,6-dimethoxyphenol (backbones of methoxyphenols) with •OH are (5.56–5.02) × 10^{-12} and (6.85–4.98) × 10^{-11} $cm^3 \cdot mol^{-1} \cdot s^{-1}$ within the range of 298–325 K, respectively, which both show a slightly negative temperature dependence (An et al., 2019, 2020). This behavior is attributed to the highly exothermic nature of •OH-initiated chemical processes including H-abstraction, OH-addition, and single electron transfer. Furthermore, VAA, VAL, and CFA are all 2-methoxyphenol congeners bearing functional substituents at the identical aromatic C position of the benzene ring. Given the similar reaction mechanisms of •OH and $SO_4^{\bullet-}$ (Herrmann et al., 2010), the possible influence of temperature on the aqueous-phase reactions of methoxyphenols is expected to be limited and not taken into account in this work.

3 Optical property analysis

At regular intervals, sample solutions were taken from the reactor and placed in a quartz cuvette with a 1 cm optical path. Deionized water was used as the reference solution. A double-beam UV-Vis spectrophotometer (M9, Shanghai Mapada, China) was employed to scan the spectra within the wavelength range of 200 nm to 800 nm, and the relationship curve between absorbance and wavelength was plotted. During data processing, the absorption spectrum signals were corrected to eliminate the background interference caused by TBA in the solution.

The fluorescence spectrophotometer (F-7000, Hitachi, Japan) was used to conduct three-dimensional excitation-emission matrix (EEM) fluorescence spectral scanning of the reaction solution. The specific parameter settings were as follows: the emission

wavelength scanning range was 220-700 nm, with a scanning step size of 5 nm; the excitation wavelength scanning range was 200-600 nm, with a scanning step size of 10 nm; the scanning speed was 2400 nm min^{-1}. Before measuring the sample solution, a blank sample was scanned to obtain the background EEM spectrum for background subtraction.

4 GC-MS analysis

The concentrations of three methoxyphenols and ferulic acid were measured by the GC-MS. A 60 mL aliquot of the reaction mixture was placed in a separatory funnel, and 20 mL of dichloromethane was added and used for extraction. Approximately 2 mL of the extract was concentrated under a nitrogen stream and transferred to a GC vial. Prior to instrument analysis, the sample was derivatized with BSTFA. The instrumental conditions were set as follows: 1 μL of sample was injected in pulse-splitless mode, with an inlet temperature of 250 °C and an interface temperature of 330 °C. The oven temperature was initially held at 80 °C for 1 minute, then increased at a rate of 15 °C·min^{-1} to 220 °C, followed by a final increase at 25 °C·min^{-1} to 300 °C, where it was maintained for 15 minutes.

5 HULIS determination

The quantification of humic-like substances (HULIS) followed the method reported by Li et al. (2022). Briefly, HULIS was isolated from reaction products using solid-phase extraction (SPE) cartridges (CNW Poly-Sery HLB). Prior to extraction, SPE cartridges were pre-rinsed sequentially with 1 mL of ultrapure water and 3 mL of

methanol. The sample solution was first acidified to pH ≈ 2 with HCl and loaded onto the SPE cartridge. The cartridge was then washed with another 1 mL of ultrapure water. HULIS was subsequently eluted with 3 mL of methanol-ammonia mixture (volume ratio, 98/2). The eluate was gently dried using high-purity N_2, which was further diluted using ultrapure water to 25 mL for HULIS quantification by the HPLC coupled with an evaporative light scattering detector (ELSD3000). Suwannee River Fulvic Acid (SRFA) served as the HULIS standard, the recovery efficiency of which was approximately 76-82% with standard deviations below 5 %.

6 Oxidation potential analysis

The specific experimental procedure was as follows: 0.5 mL of reaction solution was transferred into a 50 mL test tube, mixed thoroughly with 24 mL phosphate-buffered saline (1 mmol L^{-1}, pH 7.4) and 1 mL DTT solution (2.5 mmol L^{-1}). The tube was then placed in a 37°C water bath for the reaction. During the first hour of the reaction, 3 mL aliquots of the reaction mixture were taken every 15 minutes and mixed with 300 μL DTNB solution (5 mmol L^{-1}) in 0.1 mmol L^{-1} phosphate-buffered saline. After incubating in the dark for 5 min, the absorbance (A_t) was measured at 412 nm using UV-vis spectroscopy, where A_0 represents the initial absorbance value. In parallel, a blank control was prepared by replacing the reaction solution with 0.5 mL deionized water. Thus, the concentration of M_{DTT} in the sample could be determined through the following equation (Li et al., 2022).

$$M_{DTT}=\frac{A_0-A_t}{A_0}\times C_{DTT_0} \quad (1)$$

Here, C_{DTT0} represents the initial concentration of DTT in the sample solution, which was 98 μmol L^{-1} in this experiment. Plot the curve of M_{DTT} versus incubation time, and its slope R_{DTT} is the DTT consumption rate of the sample.

7 HR-ToF-AMS analysis and calculation of aqSOA mass yields

This study employed an Aerodyne high-resolution time-of-flight aerosol mass spectrometer (HR-ToF-AMS) to analyze the mass concentration and chemical composition of aqSOA. Notably, PDS and its reduction product sulfate undergo rapid thermal decomposition at a vaporization temperature of 600 °C, and under 70 eV electron impact ionization, they fragment into characteristic ion clusters (primarily HSO_2^+, HSO_3^+, and SO^+), which are ultimately detected by AMS as sulfate signals (Drewnick et al., 2005). Given that the concentration of organic precursors used in this experiment (0.3 mM) was significantly lower than that of PDS (50 mM), the possible formation of organic sulfur species was negligible. Based on material balance, the sulfate concentration within the system remained constant at approximately 100 mM, thus serving as an internal standard for absolute quantification correction of aqSOA. Prior to sample introduction, AMS ionization efficiency (IE) was calibrated using pure ammonium nitrate particles following standard procedures. The aqSOA mass yield (Y_{aqSOA}) refers to the ratio of the change in organic aerosol mass concentration (ΔOrg) produced during reaction time t to the change in precursor mass concentration (Δprecursor), representing the percentage of product mass formed per unit mass of precursor consumed (Ye et al., 2020). The calculation formula is shown as follows:

$$Y_{aqSOA}=\frac{\Delta Org}{\Delta precursor}=\frac{\left(m_{Org,AMS}/m_{SO_4^{2-},AMS}\right)C_{SO_4^{2-},0}}{C_0 M\eta} \quad (2)$$

In the equation, $m_{Org,AMS}$ and $m_{SO_4^{2-},AMS}$ (μg m^{-3}) represent the mass concentrations of organic aerosol and sulfate measured by HR-ToF-AMS at reaction time *t*, respectively, both corrected for dark-room background; $C_{SO_4^{2-},0}$ is the initial concentration of the internal standard (100 mM sulfate); C_0 is the initial concentration of the precursor (0.3 mM); M is the molar mass of the precursor; η is the removal efficiency, calculated as follows:

$$\eta=\frac{C_0-C_t}{C_0}\times 100\% \quad (3)$$

where C_0 and C_t are the concentrations of precursors at reaction time zero and reaction time *t*, respectively.

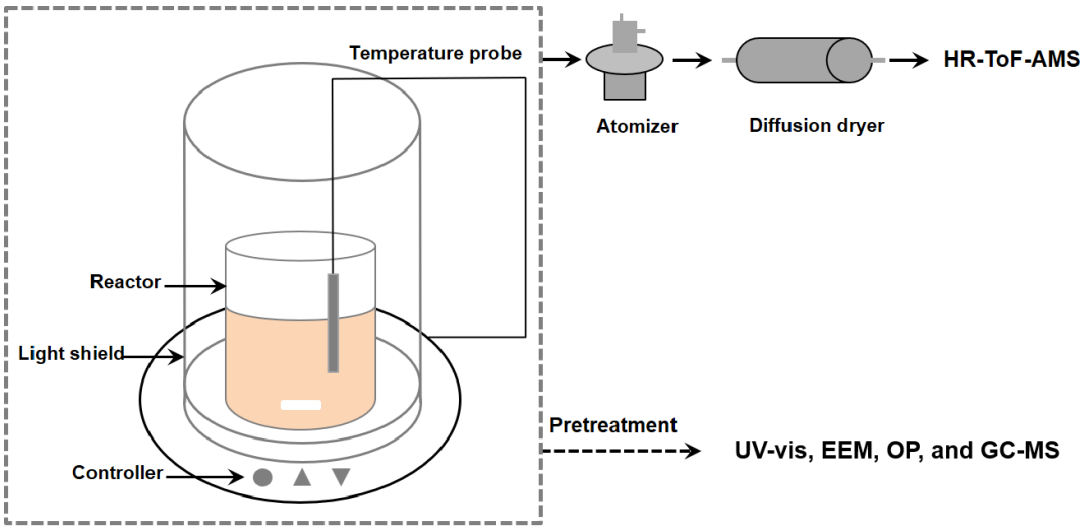

Figure S1. Schematic diagram of experimental setup.

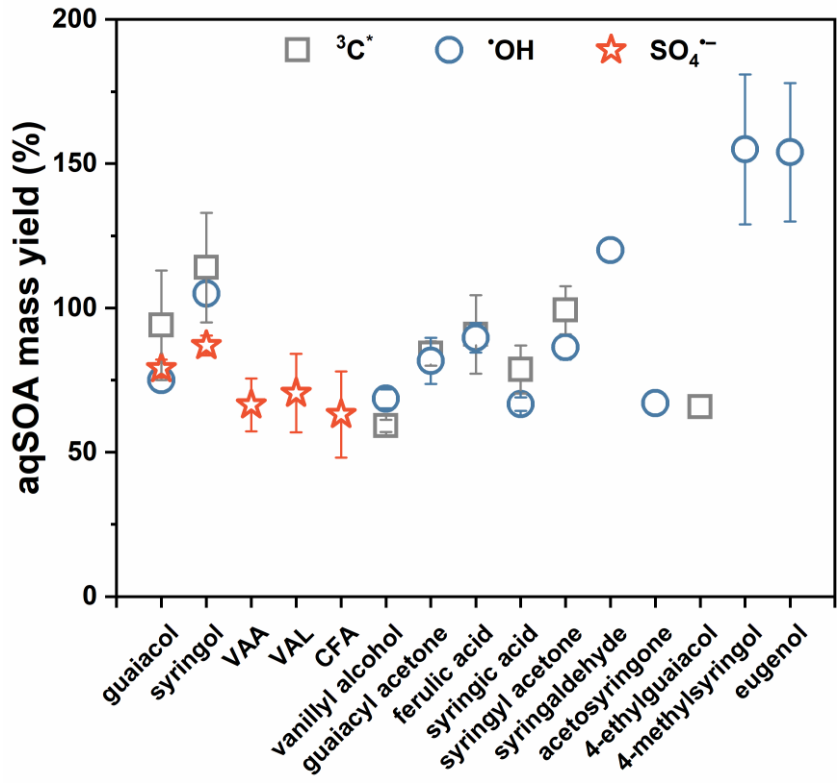

Figure S2. aqSOA mass yields of aqueous-phase reactions of methoxyphenols with $^{\bullet}OH$, $^3C^*$, and $SO_4^{\bullet-}$. Yields for vanillyl alcohol, guaiacyl acetone, ferulic acid, syringic acid, and syringyl acetone with $^3C^*$ and $^{\bullet}OH$ were from Ma et al. (2021) and Arciva et al. (2022), respectively. Yields for GUA and SYR with $^3C^*$ and $^{\bullet}OH$ were from Smith et al. (2014) and Yu et al. (2016), respectively. Yields for 4-methylsyringol and eugenol with $^{\bullet}OH$ were from Ye et al. (2020). Yield for 4-ethylguaiacol was from Chen et al. (2020). Yields for guaiacol and syringol with $SO_4^{\bullet-}$ were from Chen et al. (2026).

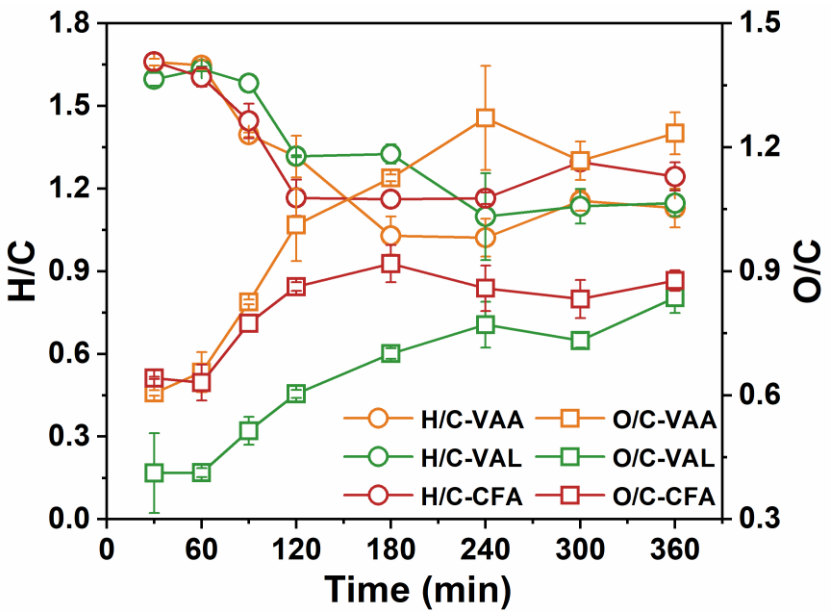

Figure S3. Variations in H/C and O/C ratios of aqSOA formed from $SO_4^{\bullet-}$-initiated aqueous-phase reactions of VAA, VAL, and CFA.

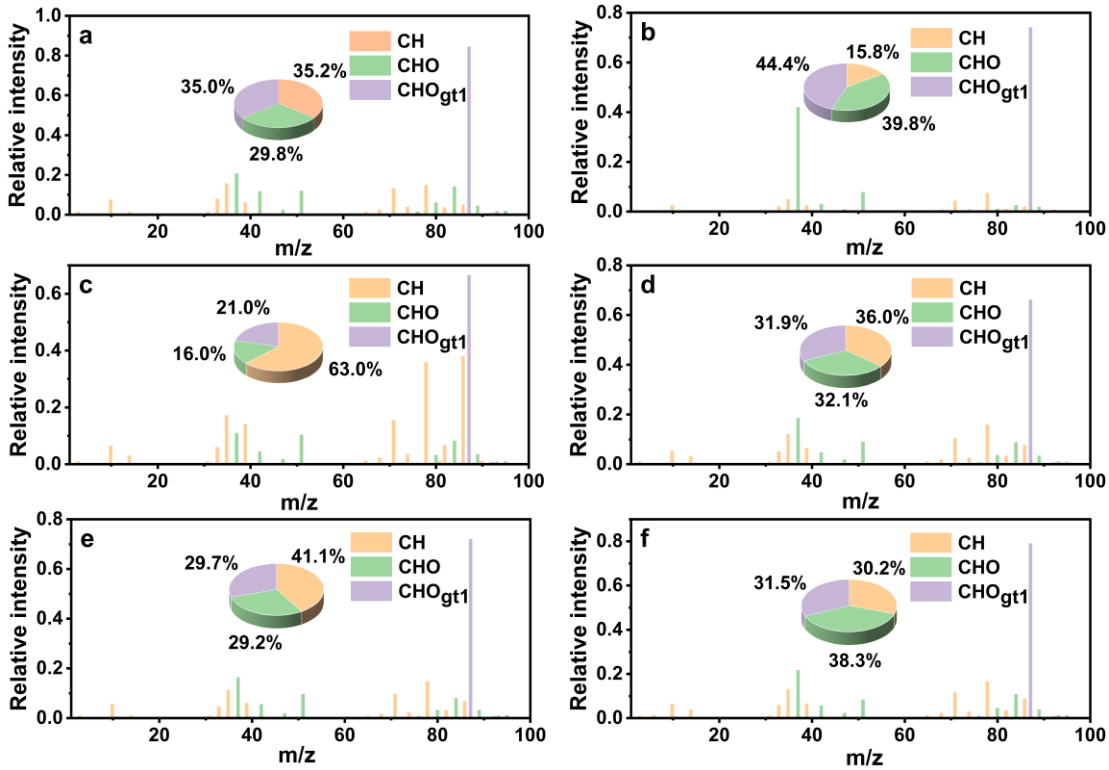

Figure S4. Mass spectra of aqSOA formed from $SO_4^{\bullet-}$-initiated aqueous-phase reactions of VAA (a and b), VAL (c and d), and CFA (e and f) at 30 min (a, c, and e) and 360 min (b, d, and f) acquired by the HR-ToF-AMS.

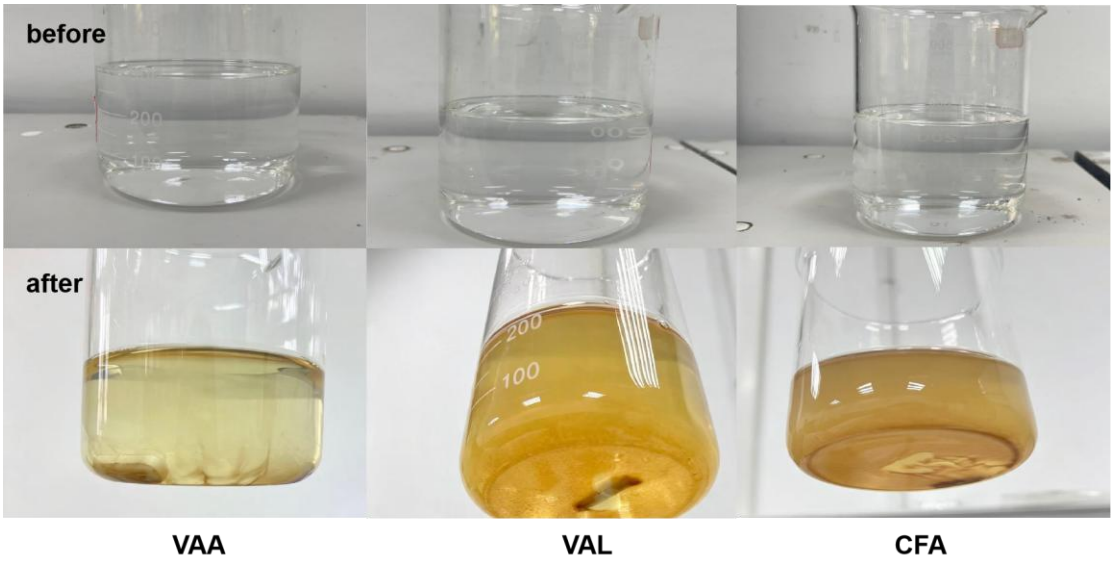

Figure S5. Variations in color of VAA, VAL, and CFA solutions before and after reactions.

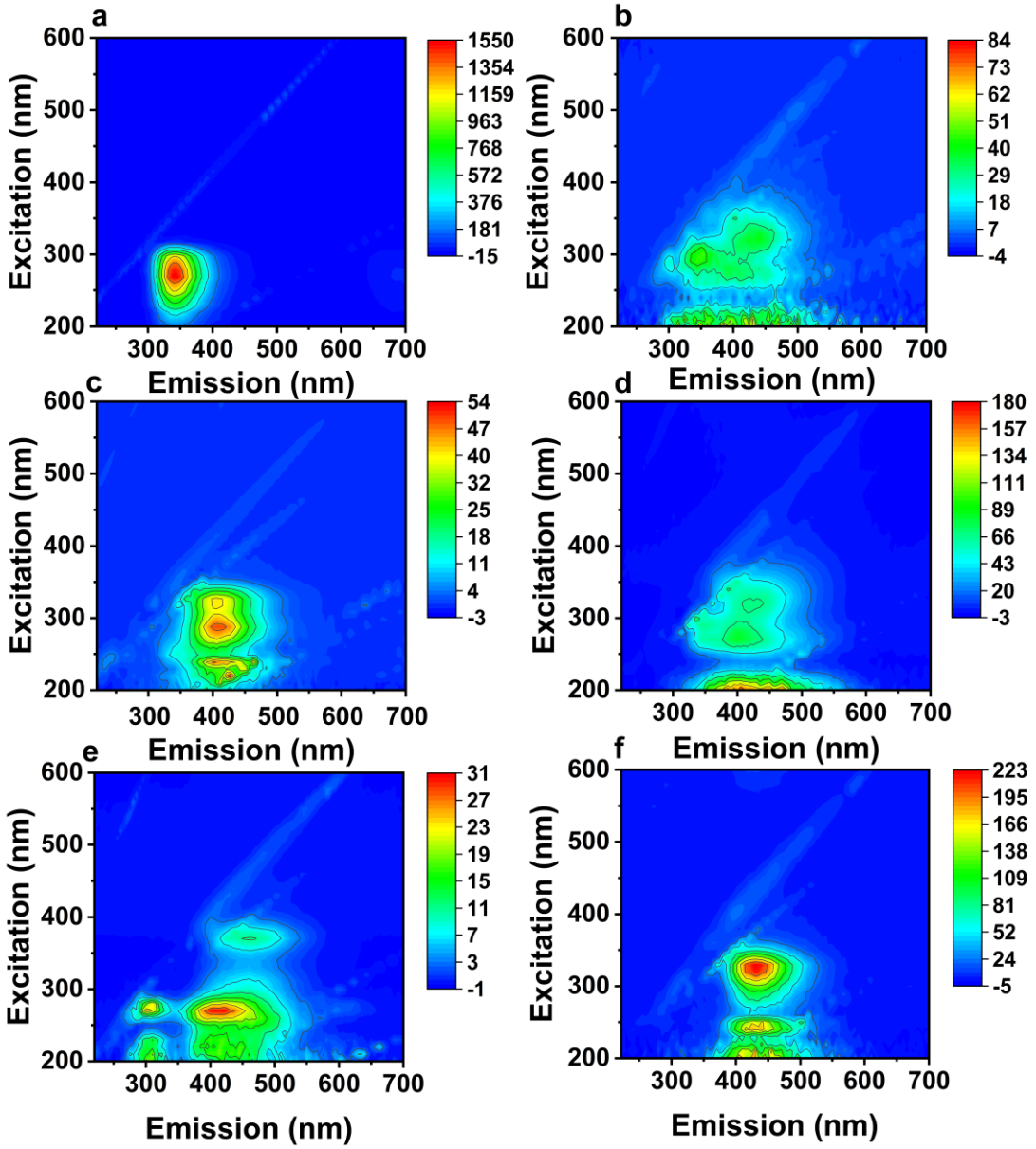

Figure S6. EEM spectra of VAA (a and b), VAL (c and d), and CFA (e and f) in the aqueous-phase reactions with $SO_4^{\bullet-}$ before (a, c, and e) and after (b, d, and f) reactions.

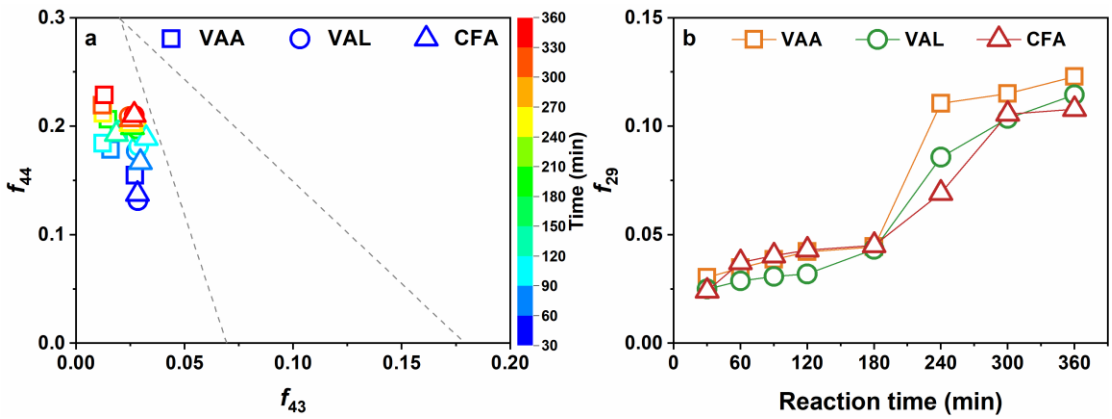

Figure S7. (a) "Triangle plots" of aqSOA formed from $SO_4^{\bullet-}$-initiated aqueous-phase reactions of VAA, VAL, and CFA, and (b) time-series variations in the organic mass fraction of m/z = 29 (f_{29}).

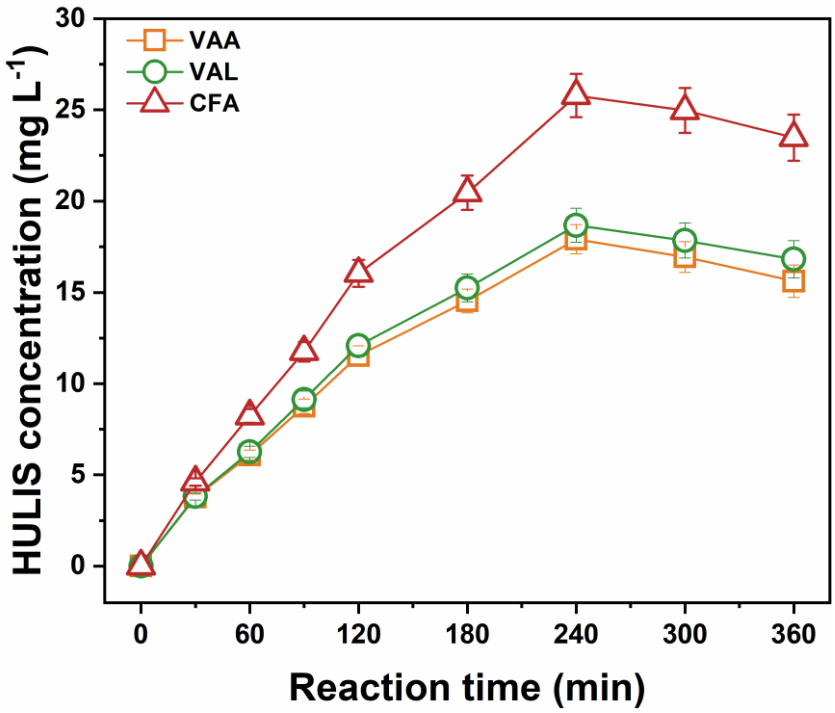

Figure S8. Time-dependent concentrations of HULIS produced in the aqueous-phase reactions of $SO_4^{\bullet-}$ with VAA, VAL, and CFA.

References

An, Z., Sun, J., Han, D., Mei, Q., Wei, B., Wang, X., and He, M.: Theoretical study on the mechanisms, kinetics and ecotoxicity assessment of OH-initiated reactions of guaiacol in atmosphere and wastewater, Sci. Total Environ., 685, 729-740, https://doi.org/10.1016/j.scitotenv.2019.06.229, 2019.

An, Z., Sun, J., Han, D., Mei, Q., Wei, B., Wang, X., Xie, J., Zhan, J., and He, M.: Effect of pH on ·OH-induced degradation progress of syringol/syringaldehyde and health effect, Chemosphere, 255, 126893, https://doi.org/10.1016/j.chemosphere.2020.126893, 2020.

Arciva, S., Niedek, C., Mavis, C., Yoon, M., Sanchez, M. E., Zhang, Q., and Anastasio, C.: Aqueous ·OH oxidation of highly substituted phenols as a source of secondary organic aerosol, Environ. Sci. Technol., 56, 9959-9967, https://doi.org/10.1021/acs.est.2c02225, 2022.

Chen, R., Li, X., Zhou, X., Chen, T., Yang, Z., Fan, L., Sun, M., Niu, Q., Liu, C., and He, H.: Sulfate radical-initiated aqueous oxidation of biomass burning tracers: a potential source of HULIS and aqSOA, Environ. Sci. Technol., 60, 9381-9391, https://doi.org/10.1021/acs.est.5c14755, 2026.

Chen, Y., Li, N., Li, X., Tao, Y., Luo, S., Zhao, Z., Ma, S., Huang, H., Chen, Y., Ye, Z., and Ge, X.: Secondary organic aerosol formation from $^{3}C^{*}$-initiated oxidation of 4-ethylguaiacol in atmospheric aqueous-phase, Sci. Total Environ., 723, 137953, https://doi.org/10.1016/j.scitotenv.2020.137953, 2020.

Cope, J. D., Bates, K. H., Tran, L. N., Abellar, K. A., and Nguyen, T. B.: Sulfur radical formation from the tropospheric irradiation of aqueous sulfate aerosols, Proc. Nat. Acad. Sci. USA, 119, e2202857119, https://doi.org/10.1073/pnas.2202857119, 2022.

Drewnick, F., Hings, S. S., DeCarlo, P., Jayne, J. T., Gonin, M., Fuhrer, K., Weimer, S., Jimenez, J. L., Demerjian, K. L., Borrmann, S., and Worsnop, D. R.: A new time-of-flight aerosol mass spectrometer (TOF-AMS)-instrument description and first field deployment, Aerosol Sci. Technol., 39, 637-658, https://doi.org/10.1080/02786820500182040, 2005.

Herrmann, H., Hoffmann, D., Schaefer, T., Bräuer, P., and Tilgner, A.: Tropospheric aqueous-phase free-radical chemistry: radical sources, spectra, reaction kinetics and prediction tools, ChemPhysChem, 11, 3796-3822, https://doi.org/10.1002/cphc.201000533, 2010.

Herrmann, H., Schaefer, T., Tilgner, A., Styler, S. A., Weller, C., Teich, M., and Otto, T.: Tropospheric aqueous-phase chemistry: kinetics, mechanisms, and its coupling to a changing gas phase, Chem. Rev., 115, 4259-4334, https://doi.org/10.1021/cr500447k, 2015.

Li, X., Tao, Y., Zhu, L., Ma, S., Luo, S., Zhao, Z., Sun, N., Ge, X., and Ye, Z.: Optical and chemical properties and oxidative potential of aqueous-phase products from OH and $^{3}C^{*}$-initiated photooxidation of eugenol, Atmos. Chem. Phys., 22, 7793-7814, https://doi.org/10.5194/acp-22-7793-2022, 2022.

Ma, L., Guzman, C., Niedek, C., Tran, T., Zhang, Q., and Anastasio, C.: Kinetics and mass yields of aqueous secondary organic aerosol from highly substituted phenols reacting with a triplet excited state, Environ. Sci. Technol., 55, 5772-5781, https://doi.org/10.1021/acs.est.1c00575, 2021.

Smith, J. D., Sio, V., Yu, L., Zhang, Q., and Anastasio, C.: Secondary organic aerosol production from aqueous reactions of atmospheric phenols with an organic triplet excited state, Environ. Sci. Technol., 48, 1049-1057, https://doi.org/10.1021/es4045715, 2014.

Ye, Z., Zhuang, Y., Chen, Y., Zhao, Z., Ma, S., Huang, H., Chen, Y., and Ge, X.: Aqueous-phase oxidation of three phenolic compounds by hydroxyl radical: insight into secondary organic aerosol formation yields, mechanisms, products and optical properties, Atmos. Environ., 223, 117240, https://doi.org/10.1016/j.atmosenv.2019.117240, 2020.

Yu, L., Smith, J., Laskin, A., George, K. M., Anastasio, C., Laskin, J., Dillner, A. M., and Zhang, Q.: Molecular transformations of phenolic SOA during photochemical aging in the aqueous phase: competition among oligomerization, functionalization, and fragmentation, Atmos. Chem. Phys., 16, 4511-4527, https://doi.org/10.5194/acp-16-4511-2016, 2016.